Advanced Bias-Free Energy Harvesting Based on High-Dielectric Flexible Electrodes With Reverse Electrowetting-on-Dielectric

Karthik Kakaraparty, *Graduate Student Member, IEEE*, Erik A. Pineda, Baylee Schumacher, Russell C. Reid, and Ifana Mahbub, *Senior Member, IEEE*

***Abstract*—A unique method for capturing energy from mechanical electrolyte modulation is known as reverse electrowetting-on-dielectric (REWOD). Prior REWOD studies relied on rigid electrodes which demand a high bias voltage to maximize harvested power, hindering the advancement of self-powered wearable health-monitoring sensors. In addition, the amount of energy harvested via the REWOD technique can be improved to a greater extent with the utilization of a high-dielectric (high-k) metal oxide (HDMO) layer on flexible electrodes. In this study, two distinct sets of electrodes that are flexible are utilized for harvesting energy with the REWOD phenomenon. The samples were coated with HDMO layers, namely, hafnium oxide (HfO_2) and manganese dioxide (MnO_2), respectively. The material deposition on a polyimide sheet is employed via a sputtering-based physical vapor deposition (PVD). The utilization of MnO_2 samples with the proposed flexing REWOD test measurement generated 476.21 μW/cm^2 an utmost power density value with an encapsulated electrolyte between electrodes.**

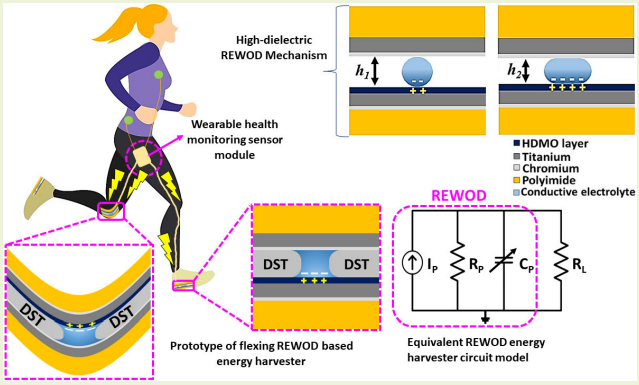

***Index Terms*— Bias-free, electro-mechanical modulation, electrolyte impingement, encapsulated electrolyte, energy harvesting, flexible electrodes, flexible reverse electrowetting-on-dielectric (REWOD), high-dielectric, REWOD.**

I. Introduction

REVERSE electrowetting-on-dielectric (REWOD) has emerged as a promising technology for energy-harvesting applications, offering the potential for self-powered systems without the need for an external bias voltage. Electrowetting, a well-studied phenomenon, involves the variation in surface tension of an electrolyte on a planar structure when an electric field is applied [1], [2], [3]. Electrowetting-on-dielectric (EWOD) is the term used to describe electrowetting that occurs on a dielectrically isolated surface, and it has found diverse applications. However, a seminal work by Krupenkin and Taylor [4] introduced the concept of reversing the premise of EWOD by harnessing the mechanical modulation of liquid droplets for electrostatic energy creation, giving rise to the REWOD phenomenon. This intriguing phenomenon has attracted considerable attention from researchers, with numerous recent studies exploring its potential for energy harvesting from electrolyte impingement [5], [6], [7]. The advancement of healthcare monitoring, particularly in wearable and implantable sensors, has revolutionized the field of human health tracking [8], [9], [10], [11]. Wearable technology has enabled continuous monitoring of various health parameters, offering valuable real-time data for clinicians [12], [13], [14], [15]. However, traditional wearable sensors rely on batteries, which present limitations in terms of device longevity, performance, and safety concerns associated with battery replacements and electrolyte leakage [16], [17], [18], [19], [20]. To overcome these limitations, energy-harvesting technologies have been explored as alternatives. Triboelectric nanogenerators (TENG) exhibit potential within the lower frequency spectrum but suffer from mechanical degradation. It is to be noted that TENG harnesses the triboelectric

Manuscript received 11 November 2023; revised 18 December 2023; accepted 18 December 2023. Date of publication 22 February 2024; date of current version 2 April 2024. This work was supported by the National Science Foundation (NSF), under Grant ECCS 2246559. The associate editor coordinating the review of this article and approving it for publication was Prof. Kai Wu. *(Corresponding author: Ifana Mahbub.)*

Karthik Kakaraparty and Ifana Mahbub are with the Department of Electrical and Computer Science Engineering, The University of Texas at Dallas, Richardson, TX 75080 USA (e-mail: Karthikeya.Kakaraparty@UTDallas.edu; ifana.mahbub@utdallas.edu).

Erik A. Pineda is with The University of Texas at Dallas, Richardson, TX 75080 USA.

Baylee Schumacher and Russell C. Reid are with the Department of Engineering, Utah Tech University, St. George, UT 84770 USA.

Digital Object Identifier 10.1109/JSEN.2023.3345841

phenomenon, wherein electricity is generated when two materials come into contact and subsequently separate. This generation occurs as a result of electron transfer driven by variations in their electronegativities [21], [22], [23], [24]. This specific mechanism, which entails material contact and separation, is fundamentally different from the REWOD approach. REWOD predominantly relies on the mechanical modulation of an electrolyte and subsequent alterations in capacitance without direct electrode–electrode interaction. There is an electrolyte bridge between two electrodes, and the REWOD energy generator relies fully on the electrolyte modulation mechanism.

Additionally, other techniques, such as electromagnetic and piezoelectric approaches, face challenges in terms of the frequency range, material degradation, and radiation safety concerns [25], [26], [27], [28]. In light of the limitations of existing energy-harvesting technologies [29], [30], [31], [32], [33], [34], there is a critical need for a reliable and long-lasting energy harvester that operates in a low-frequency range (1–5 Hz). REWOD, based on its unique electrostatic energy-harvesting mechanism, has emerged as a potential solution. Unlike other techniques, REWOD is independent of solid structure resonance, making it suitable for low-frequency applications. Additionally, the enhancement of design resilience and relaxation of spatial constraints are achieved through the incorporation of multiple electrodes, each with a two-drain architecture for a solitary energy collector [35], [36]. A mechanical force is applied to the electrolyte between conductive and dielectric electrodes and as such the REWOD generates voltage through variations in electrical capacitance. The periodic impingement of the electrolyte under external mechanical force enables the mechanical energy of the modulated electrolyte to convert into electrical energy. The REWOD mechanism notably has shown successful operation at low frequencies, offering promising prospects for capturing energy through physical human activity. In addition, to enhance energy harvesting and improve system effectiveness in REWOD, it is crucial to investigate the impact of high-dielectric (k) metal-oxide (HfO_2 and MnO_2) coating on flexible electrodes. These coatings have shown the potential to significantly increase the harvested energy by enhancing voltage generation during the REWOD process. Our research explores the potential of REWOD-based energy harvesting with flexible electrodes. In our initial investigation, we successfully demonstrated the flexibility of the REWOD-based approach without the need for a bias voltage. Building upon this, our subsequent exploration focused on incorporating high-dielectric materials into a flexible REWOD device. This innovative integration has proven to significantly enhance current and power outputs, surpassing those of other zero-bias REWOD devices. The outcomes of this study position us at the forefront of advancing applications in flexible REWOD energy harvesting, laying a foundation for cutting-edge technologies in the near future. Therefore, conducting a comparative study to explore the effectiveness of high-k metal oxide layers is essential for advancing REWOD-based energy harvesting and unlocking its substantial potential.

II. Experimental Section

A. Flexible Electrode Fabrication

The fabrication process involves the utilization of a polyimide sheet to create electrodes of two separate kinds. The selection of a 0.1-mm-thick polyimide sheet is based on its flexible nature. The sheet is divided into 12 equal-sized portions, each with an area of 35×35 mm^2. Among these portions, six are coated with chromium (Cr) and titanium (Ti) layers, each with 50- and 150-nm thickness, respectively. For the remaining six samples, in addition to the Cr and Ti layers, high-dielectric materials, specifically HfO_2 (dielectric value (κ) $\cong$ 25) and MnO_2 (dielectric value (κ) $\cong$ 101), are applied with a thickness of 100 nm each. It is important to note that the HfO_2 and MnO_2 coatings were individually applied to separate sets of samples for subsequent comparison. The deposition of these coatings onto the polyimide sheet is achieved using a sputtering-based physical vapor deposition (PVD) technique. The two-layer coated samples without dielectric coating serve as the top electrode, while the previously described three-layer coated samples with the dielectric layer are used as the bottom electrode.

The sputtering-based EBPVD material coating is executed through the advanced AJA 1500 sputter system, manufactured by AJA International. The material characterization involved a meticulous approach for four distinct materials: chromium (Cr), titanium (Ti), hafnium dioxide (HfO_2), and manganese dioxide (MnO_2). For chromium (Cr), a precisely calibrated 50-nm coating was achieved with a 40% power setting from a 500-W source (equivalent to 200 W), under the vigilant control of a deposition pressure set at 5 milli-Torr (mT). The sputtering process was thoughtfully propelled by an argon gas flow rate of 20 standard cubic centimeters per minute (sccm), and the target-to-substrate distance was meticulously maintained at 60 mm to ensure uniformity. A deposition rate of 6.84 nm/min was meticulously upheld, ultimately yielding a pristine Cr coating atop a polyimide sheet substrate. Titanium (Ti) was subjected to a highly precise sputter deposition process resulting in a 150-nm coating. This level of control was realized with a 30% power setting of the 500-W source (equivalent to 150 W) and a controlled deposition pressure of 3 mT. The argon gas flow rate, set at 20 sccm, was conscientiously maintained throughout the process, and the target-to-substrate distance was sustained at 60 mm to ensure uniformity. A deposition rate of 3.45 nm/min was vigilantly regulated, culminating in a high-quality Ti coating on top of Cr coating. For the HfO_2 samples, hafnium dioxide (HfO_2) measuring 100 nm in thickness, was attained with a power setting of 80% from the 500-W source (equivalent to 400 W) under a precisely regulated deposition pressure of 10 mT. A carefully controlled argon gas flow rate of 30 sccm facilitated the sputtering process. The target-to-substrate distance upheld at 80 mm, assured precision and uniformity in coating distribution. With a deposition rate of 7.5 nm/min, an impeccable HfO_2 coating was meticulously deposited on top of the Ti coating. For the MnO_2 samples, a manganese dioxide (MnO_2) coating, meticulously set at 100 nm in thickness, was achieved through a carefully controlled process. A power setting of

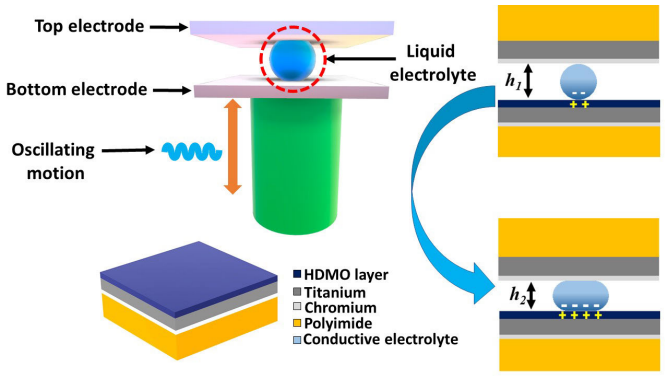

Fig. 1. Fundamental REWOD process visualization wherein displacement of the electrodes owing to the impingement of the electrolyte is expressed as $\Delta h = h_1 - h_2$.

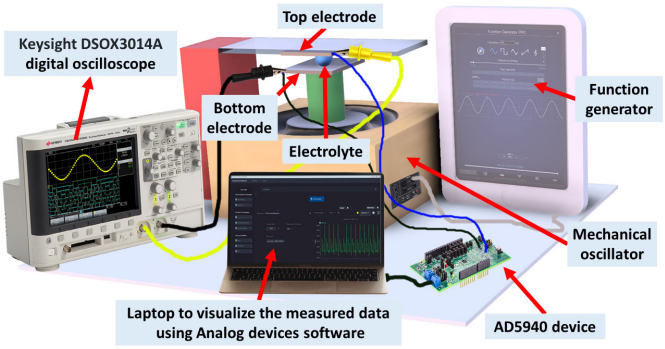

Fig. 2. Graphical illustration of the measurement system for the REWOD energy harvester in the configuration where the electrodes are maintained parallel with each other.

70% from the 500-W source (equivalent to 350 W) was finely adjusted, in conjunction with a controlled deposition pressure of 8 mT. The argon gas flow rate, set at 25 sccm, was precisely monitored. The target-to-substrate distance was consistently maintained at 70 mm, ensuring uniformity in the coating distribution. With a deposition rate of 6.0 nm/min, a highly precise and well-defined MnO_2 coating was meticulously achieved on top of Ti coating. A trinocular stereo microscope (AmScope 1140) is employed for visual inspection to ensure the consistency of the coating after the deposition process is completed. Additionally, an in situ scanning electron microscope (SEM) nanomechanical instrument, Hysitron PI 89 SEM PicoIndenter, is utilized to precisely estimate the overall coating thickness.

B. Measurement Setup

The depiction in Fig. 1 effectively illustrates the pivotal role of the electrolyte impingement mechanism in the REWOD process. The measurement setup is graphically visualized and depicted in Fig. 2. A 50-μL volume of pure deionized water is employed as the electrolyte and positioned between the top and bottom flexible electrodes. The bottom electrode is supported by a stand and placed on a mechanical oscillator to facilitate vertical displacements, while the top electrode remains fixed. Fig. 3(a) illustrates the electrolyte modulation effect, leading to charge generation at electrolyte–electrode interfaces, and Fig. 3(b) shows its equivalent lumped element circuit representation as presented in our prior work [1].

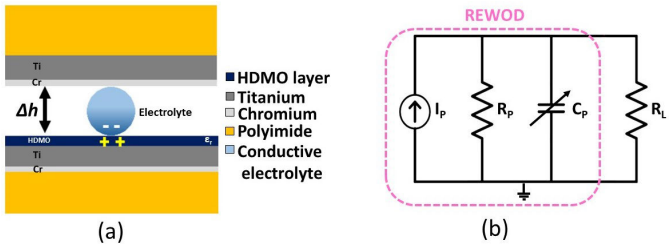

Fig. 3. Parallel configuration and lumped element model of the REWOD energy harvester. (a) Cross-sectional view of REWOD configuration. (b) Equivalent lumped element model for parallel configuration REWOD.

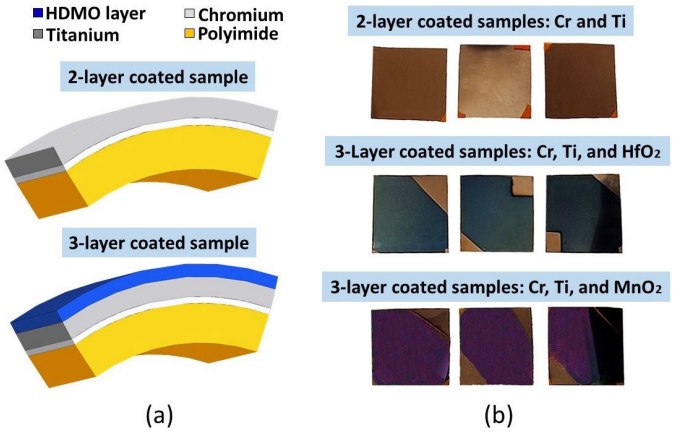

Fig. 4. Flexible sample with three-layer coating. (a) Illustrative visualization. (b) Fabricated flexible samples utilized in the REWOD experiment.

The components of the parallel setup are a resistor (R_P), a variable capacitor (C_P), a variable current source (I_P), and a load (R_L). The variation in the capacitance between the top and bottom electrodes is represented by a variable capacitor (C_P), resistance generated across the electrolyte–electrode interface is (R_P), and I_P represents the generated alternating current on the REWOD electrodes. Factors such as electrical conductivity, the distance variation of the electrode–electrolyte interface, as well as the electrolyte modulation, all contribute to C_P to behave as a capacitor whose value varies over time. Fig. 4(a) portrays a graphical representation of two-layer metals-only coated samples and three-layer coated samples with a high-dielectric metal-oxide layer, and Fig. 4(b) presents the fabricated flexible samples, portraying metal contacts at the edges of the three-layer coated samples to facilitate connections for the collector and ground probe during measurements.

Oscillation frequencies ranging from 1 to 5 Hz are applied to the mechanical oscillator using a mobile or iPad-controlled frequency generator application. During the electrolyte impingement process, ac peak-to-peak voltage recordings are measured using a Keysight oscilloscope (DS0$\times$ 3014A). Fig. 5(a) presents the REWOD measurement setup for harvesting energy, and Fig. 5(b) shows the electrolyte bridge between the top and bottom electrode configuration, the bottom electrode is placed on a support stand which is attached to a mechanical oscillator. Fig. 5(c) portrays the collector and ground probes connected to the metal contacts of the top and bottom electrodes. The collector probe is connected to the top electrode, while the ground probe is connected to the bottom electrode. Furthermore, the collector and ground probes are

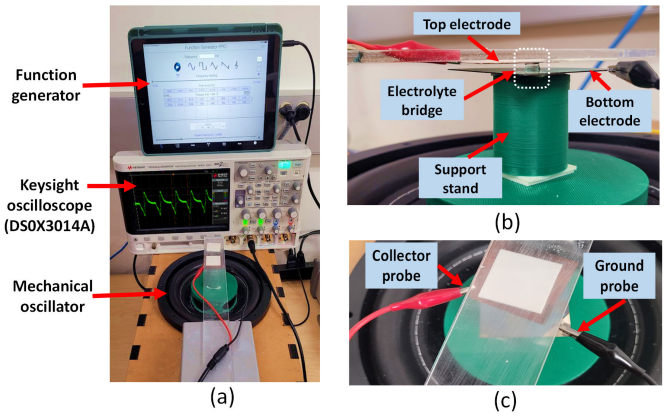

Fig. 5. (a) Energy-harvesting REWOD measurement configuration. (b) Side-wise picture portraying the droplet bridge between the top and bottom electrodes. (c) Top view showing the ground and collector connections.

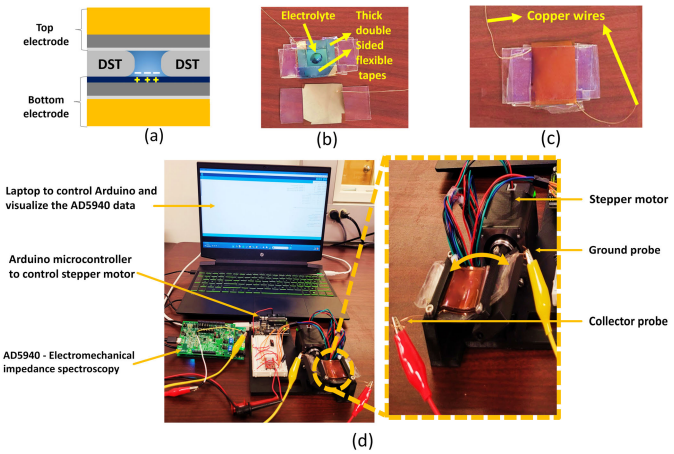

Fig. 6. Preparation of flexing samples. (a) Visualization of the cross section of the REWOD flexing sample. (b) Placement of the electrolyte into the slot created by DST. (c) Copper wire extensions to the enclosed flexing sample. (d) Final REWOD flexing test configuration.

connected to an impedance analyzer (AD5940) to analyze resistance and capacitance variations resulting from changes in the surface area caused by the electrolyte impingement procedure.

III. Flexing Experiment for Electrodes

The two-layer (Cr and Ti) and three-layer (Cr, Ti, and HDMO) coated fabricated flexible samples were subjected to a bending test with a special 3-D printed fixture that is designed to bend the samples. The objective was to evaluate the durability and resilience of the coated layers applied to the polyimide substrate. Subsequent to the bending test, a visual inspection was conducted on the flexible electrodes. Remarkably, the coating on the polyimide substrate exhibited no signs of deterioration, even after undergoing multiple bending cycles. To execute the flexing REWOD examination, a setup was established involving a stepper motor, an Arduino microcontroller board, and a 3-D-printed model incorporating a manipulable pedal. The 3-D-printed configuration included a support structure to secure the stepper motor and an adjustable pedal affixed to the arm of the motor. During the evaluation, the flexible electrode was positioned on the apparatus, and the Arduino microcontroller was employed to command the stepper motor's motion. The motor's rotation spanned from 0° to 90°, and potentially beyond. The stepper motor, interconnected with an Arduino microcontroller, is controlled via programed instructions. The extent to which the motor should be rotated is instructed via a straightforward Arduino program that is preloaded in the microcontroller which takes the input value starting from 0° to 360°. The program pertains the motor's rotation extent to the input provided.

The flexing REWOD test sample consists of top and bottom electrodes that are sealed together with an electrolyte situated inside the enclosed space. The top and bottom flexible electrodes were each independently linked to two copper wires that were extended outward which served as the collector and ground terminals, respectively. Fig. 6(a) portrays a cross-sectional illustration of electrolyte confinement within the flexing test sample. The lower electrode's conductive portion is connected to a copper wire and securely bonded using epoxy, which undergoes a curing process lasting 24 h. Around the lower electrode, a double-sided tape (DST) serves as a support structure to contain the electrolyte, as shown in Fig. 6(b). The boundary of DST is subsequently coated with UV-curable adhesive and cured by exposure to UV light to ensure a proper seal. Once the adhesive has solidified, a 50-μL electrolyte is introduced into the space enclosed by the DST. Similarly, the upper electrode is connected to a copper wire in a manner resembling the lower electrode. To establish a complete seal and prevent electrolyte leakage, the uncoated side of the upper electrode is affixed with a larger DST. This arrangement positions the coated side of the upper electrode to fully enclose the space between the two electrodes, as illustrated in Fig. 6(c). The bend test sample is supported on the aforementioned 3-D printed structure as demonstrated in Fig. 6(d).

IV. Results and Discussion

A. AC Voltage Measurements

The ac voltage generated by the REWOD setup was measured using a Keysight oscilloscope (DS0 × 3014A) and analyzed using the Analog Devices software. The measurements were conducted within a frequency range of 1–5 Hz with a step size of 1 Hz. An almost linear relationship was observed between the ac peak-to-peak voltage and frequency. The samples coated with an HfO_2 metal-oxide layer produced ac voltage values with the REWOD set up in the range of 526–934 mV. A 50-μL electrolyte with 0.33-cm^2 interfacial area between the electrode and the electrolyte with a 2-mm displacement variation between the electrodes was utilized to obtain these voltage ranges for all three considered flexible electrodes. Similarly, the samples coated with MnO_2 generated ac voltages in the range of 1034 V–2002 mV. Fig. 7 presents all the voltage plots. Specifically, Fig. 7(a) corresponds to voltage variation versus frequency for nonbending REWOD measurement with HfO_2 samples, and Fig. 7(b) corresponds to voltage variation in the time domain for a 1-s interval. Similarly, Fig. 7(c) and (d) corresponds to nonbending

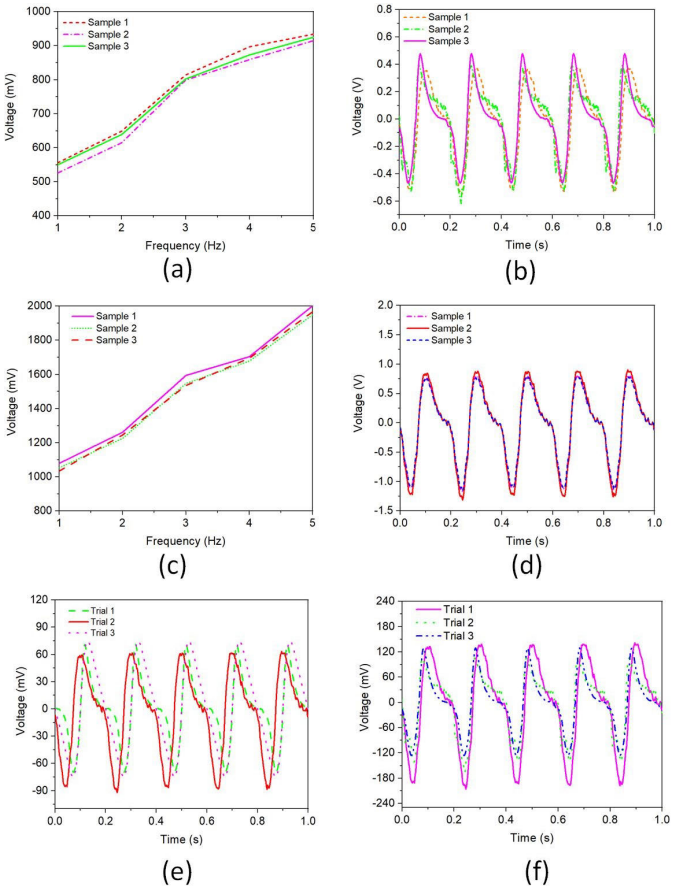

Fig. 7. Voltage plots in the time and frequency domains. (a) and (b) In the case of HfO_2 utilized as an HDMO layer. (c) and (d) In the case of MnO_2 utilized as an HDMO layer. (e) Three flexing test trials with the HfO_2 sample at 5-Hz modulation frequency. (f) Three flexing test trials with the MnO_2 sample at 5-Hz modulation frequency.

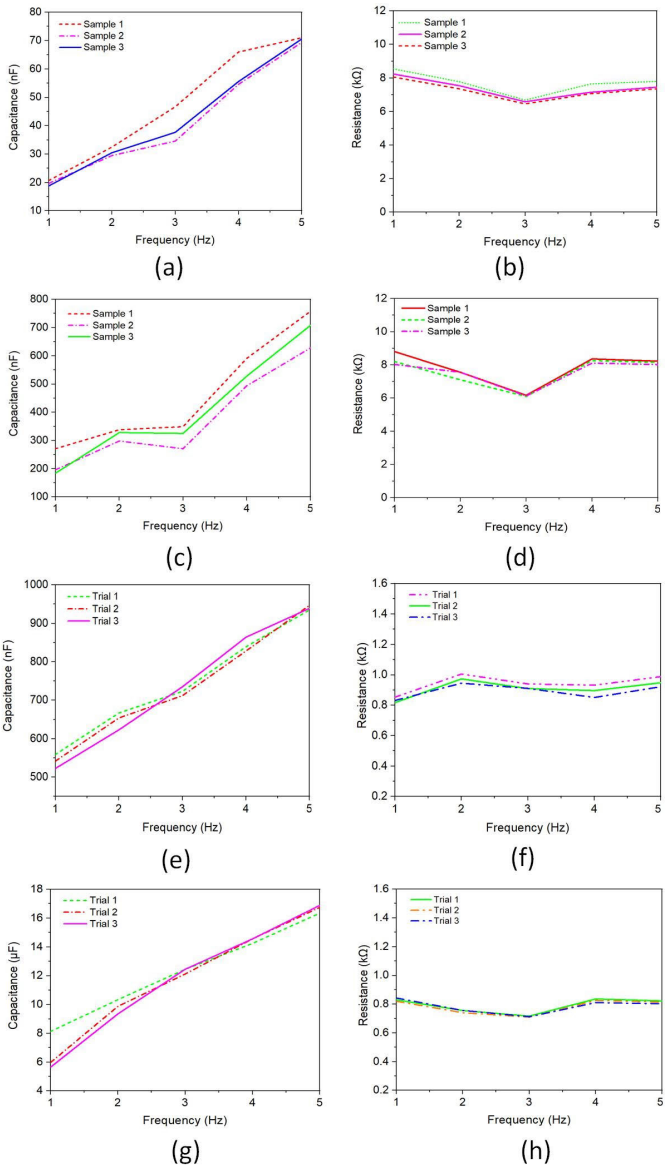

Fig. 8. RC variation over frequency: (a) and (b) HfO_2 with conventional REWOD, (c) and (d) MnO_2 with conventional REWOD, (e) and (f) flexing test with the HfO_2 sample, and (g) and (h) flexing test with the MnO_2 sample.

REWOD measurements with MnO_2 samples. Fig. 7(e) shows the three voltage test trials with HfO_2 samples based on the flexing REWOD test, and Fig. 7(f) presents three voltage test trials with MnO_2 samples based on the flexing REWOD test. It is observed that the voltage plots followed an increased trend starting from 1 to 5 Hz in the nonbending REWOD experiments. The flexing test trials exhibited a remarkable degree of similarity across all three trials conducted for both HfO_2 and MnO_2 samples.

B. RC Measurements

The REWOD system model comprises a current source represented by I_P and is accompanied by parallel capacitance C_P and resistance R_P. The presence of electrical resistance R_P between the electrodes is influenced by various factors, including the conductivity of the electrolyte, electrolyte thickness, displacement between the two electrodes, conductive and dielectric layers, and the electrode–electrolyte interfacial area. During the electrolyte impingement process, the analog front-end device AD5940 measures the overall impedance magnitude ($|Z|$) and phase angle (Φ) of the system.

R_P and C_P indicate the system's resistance and capacitance, respectively, which are estimated utilizing (1) and (2). The absolute impedance ($|Z|$) is given as in (3) and $\omega = 2\pi f$ represents the oscillation frequency of the ac signal, as previously detailed in our earlier work [1].

The variation plots for all the RC measurements are depicted in Fig. 8. Specifically, Fig. 8(a) and (b) represents HfO_2 with the nonbending REWOD setup, while Fig. 8(c) and (d) corresponds to MnO_2 with the nonbending REWOD setup. Fig. 8(e) and (f) corresponds to trials carried out with the HfO_2 sample based on the flexing REWOD test, and likewise, Fig. 8(g) and (h) corresponds to flexing test trials with the MnO_2 sample. Notably, it is observed that the resistance values measured during the bend test trials were consistently lower than those attained through the nonbending REWOD setup. In contrast, the capacitance values exhibited an increased trend when subjected to the bend test. The capacitance increase in the flexing test might be attributed to the reduced distance between the electrodes in the bend test as compared to the nonbending REWOD test configuration.

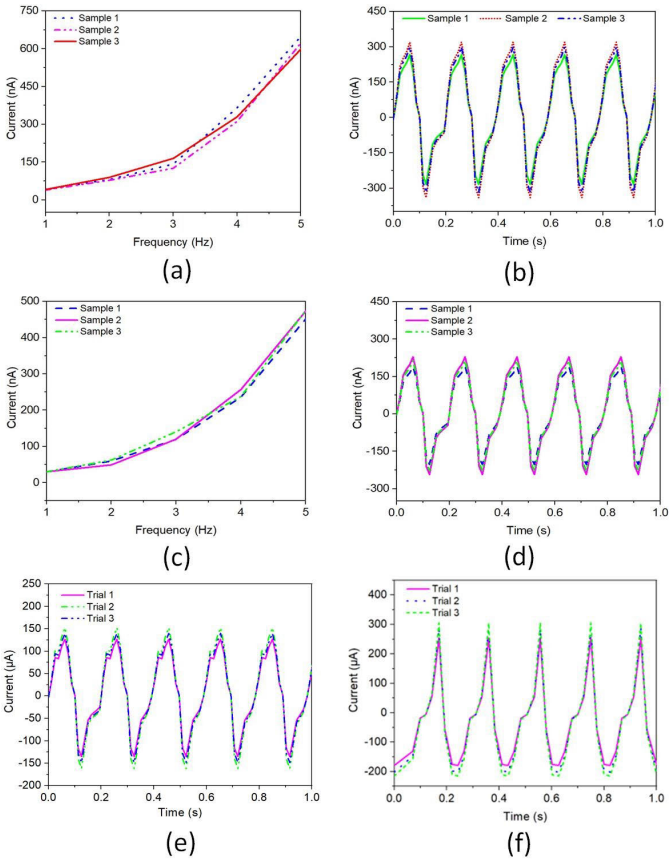

Fig. 9. Current plots in the time and frequency domains. (a) and (b) In the case of HfO_2 utilized as an HDMO layer. (c) and (d) In the case of MnO_2 utilized as an HDMO layer. (e) Three flexing test trials with the HfO_2 sample at 5-Hz modulation frequency. (f) Three flexing test trials with the MnO_2 sample at 5-Hz modulation frequency.

For all three flexible electrodes in each case scenario, the capacitance and resistance values were almost similar and followed the same pattern. The capacitance generated with the HfO_2 samples ranged from 18 to 71 nF for the frequency range of 1–5 Hz, similarly, with the MnO_2 samples generated capacitance ranged from 184 to 758 nF. It is observed that the capacitance generated with the MnO_2 coated samples has ≈10.5 times higher capacitance generation when compared to the HfO_2 coated samples. The peak-to-peak ac current with the HfO_2 samples generated by the conventional REWOD setup is 471.37 nA and that of MnO_2 samples is 659.92 nA. However, the resistance measured across the top and bottom electrodes for the considered samples needs to be essentially the same in each case scenario because all of the flexible electrodes employed have the same metal covering, and the RC measurements supported this notion

$$R_P = \frac{\tan(\Phi)}{\omega C_p} \tag{1}$$

$$C_P = \frac{\tan(\Phi)}{\sqrt{\left(\frac{1}{R_P}\right)^2 + (C_p\omega)^2} \times |Z| \times \omega} \tag{2}$$

$$|Z| = \frac{1}{\sqrt{(\omega C_p)^2 + \left(\frac{1}{R_P}\right)^2}}. \tag{3}$$

C. Flexing Test Measurements

The utilization of HfO_2 as an HDMO layer with REWOD flexing configuration has generated 45.27 μW of power with a voltage maximum of 155 mV between the peaks and 292 μA of current maximum between alternating peaks at a 5-Hz frequency of operation. Similarly, the MnO_2 samples generated a 310 mV of voltage maximum and 507 μA of current maximum values resulting in 157.15 μW of power. This might activate the wearable biosensors with typical nanowatt level power requirement [41]. The power density produced during the flexing test is around 118 times more than in the scenario with flexible electrodes with the typical REWOD configuration. This is observed as the flexing REWOD test yielding a relatively low resistance value of 1 kΩ at 5 Hz compared to the 7-kΩ resistance observed in the nonbending REWOD planar structure scenario. Furthermore, the flexing REWOD test generated a capacitance of 16.89 μF, approximately 21 times greater than the 758-nF capacitance generated with the standard REWOD setup, which is the primary factor contributing to the higher current observed during the bending test. The elevated capacitance observed during the bending test leads to a corresponding increase in current, and this heightened current is the primary contributor to the augmented power generation in the bend test owing to $P = V \times I$, where the power generated is directly proportional to the ac current produced. Also, in the flexing measurement, the separation between electrodes lies within the range of 0.5–1 mm. This distance is four times closer than the electrode distances in the typical REWOD setup scenario, where the distances range from 2 to 4 mm. This resulted in the electrode and the electrolyte having a larger surface area in contact during the bending experiment, which may also be accountable for the enhanced capacitance generation, leading to a subsequent increase in current and eventually greater power generation. As the distance between the electrodes decreases, it is anticipated that the capacitance between them will rise, and this expectation aligns with the corresponding measurements of resistance (R) and capacitance (C). Higher power density generation in the flexing REWOD test case has been supported by all of the aforementioned factors.

The current generated with HfO_2-coated samples in the flexible bend test is ≈103 times greater than the current produced by a typical REWOD setup in which the samples were not bent. Similarly, it is observed that the flexing test with MnO_2 samples generated ≈118 times more in comparison with the standard REWOD test. The elevated current magnitude observed during the bend-test scenario is the principal contributor to the increased power generation in this specific configuration.

The present study is compared with related previous studies by taking into account the parameters listed in Table I, comprising the type of energy harvester, maximum frequency modulated, externally applied bias voltage, and power density (μW/cm^2). The flexing REWOD proposed in this work operates in the range of 1–5 Hz. Although Krupenkin et al. [4] and Yang et al. [6] demonstrate that their energy-harvesting mechanism can produce ultrahigh power densities, it was implemented with the utilization of comparatively high bias

TABLE I
COMPARISON WITH EARLIER STUDIES

References	Dielectrics-utilized	Droplets-utilized	Droplet volume (μL)	Modulation Frequency [Hz]	Bias-voltage [V]	Electrolyte-utilized	Power-density [$\mu W/cm^2$]
Krupenkin *et al.* [4]	Ta_2O_5	150	50	2	60	Mercury (Hg)	10,000
Yang *et al.* [6]	Al_2O_3	1	50	3	24	Mercury (Hg)	10,960
Hsu *et al.* [37]	Ta_2O_5	16	100	300	4.5	Mercury (Hg)	10,000
Huynh *et al.* [38]	TiO_2	1	20	6	1.2	NaCl solution	0.096
Adhikari *et al.* [1]	Al_2O_3	1	50	5	No bias voltage	deionized water	3.18
Adhikari *et al.* [39]	Al_2O_3	1	50	5	No bias voltage	deionized water	0.075
Kakaraparty *et al.* [40]	Al_2O_3	1	50	5	No bias voltage	deionized water	*0.002 and **0.050
This work	MnO_2 and HfO_2	1	50	5	No bias voltage	deionized water	*4.01 and **476.21

*REWOD-planar. **REWOD-flexible.

voltages in earlier works that made this possible. In [1], the REWOD energy-harvesting procedure utilized rigid and rough electrodes. Although it demonstrated a 3.18 μW/cm^2 of high power density, the limitation lies in the fact that these rigid electrodes cannot support the scalability of research for energy harvesting through human motion, due to structural constraints. The REWOD harvester comprises a top electrode, a bottom electrode, and an electrolyte (deionized water in this work) in between both electrodes. Energy is generated through mechanical modulation of the electrolyte, which varies the electrolyte–electrode interfacial area and thus creates capacitance variation. As a result, it generates alternating current and alternating voltage between both electrodes and thus the power is generated. The harvested power is intended to be temporarily stored in a capacitor, and once a sufficient energy level is attained, it is envisioned to be transferred via connected wires to a wearable biosensor to activate it. This innovative approach envisions the placement of a flexing sample within the shoe sole, strategically harnessing human pressure during walking to induce modulation of deionized water confined between top and bottom electrodes. This orchestrated movement activates the REWOD mechanism, paving the way for efficient energy harvesting. In this envisaged scenario, the connected wearable sensor draws its power from this ingeniously integrated REWOD mechanism, illustrating the potential of a symbiotic relationship between energy-harvesting and biosensing technologies. This innovative, self-sustaining energy-harvesting technique substantially reduces the need for frequent battery replacements, representing a noteworthy advancement in sustainable technology. Therefore, there is a critical need to employ flexing electrodes to pave the way to flexible bias-free REWOD-based energy generation research. Previous work utilized a PDMS substrate, which is flexible but lacks thermal stability compared to the polyimide substrate used in our study. Furthermore, the utilization of PDMS substrate in earlier research resulted in some inconsistency in coating with EBPVD technique [39].

Huynh et al. employed 1.2 V of external voltage bias to achieve a 0.096-μW/cm^2 power density value in their research. In contrast, our study achieved a power density of 4.01 μW/cm^2 with the conventional REWOD system with the MnO_2 sample for a modulation frequency of 5 Hz with an electrode displacement of 2 mm, without utilization of any bias voltage, utilizing an electrode–electrolyte interface area of 0.33 cm^2. Our flexible electrode-based REWOD flexing test, featuring a 65° bend angle, yielded an electrode–electrolyte interface area of approximately 1.2 cm^2, and the estimated power density is 476.21 μW/cm^2.

Unlike prior research which utilized a polydimethylsiloxane (PDMS) substrate, this study employs a Kapton polyimide substrate with electron beam PVD (EBPVD) coating. Visual examination under an AmScope 1140 microscope revealed superior coating uniformity compared to 3-D-printed PDMS. Kapton was chosen for its high thermal stability (>200 °C) during EBPVD. We simplified the fabrication process by eliminating the need for an extra 3-D ink printing stage, making the procedure more efficient [39].

REWOD measurements are devoid of direct electrical connections to data probes. ac voltage and current data are tied to electrolyte modulation. The Keithley Series-2400 tool offers precise measurements in all four quadrants with noise filters, ensuring low noise and high accuracy. This eliminates the electrical noise in Figs. 7(b)–(f) and Figs. 9(b)–(f).

The power density achieved utilizing the MnO_2 samples with the conventional REWOD is ≈9 times higher than that of the value generated with HfO_2, and ≈2K times greater than our prior work with Al_2O_3 [40]. In addition, for the flexing test case, the MnO_2 samples harvested power density ≈3.5 higher than the HfO_2 case, and ≈9.5K times greater than the aforementioned Al_2O_3 case. The comparison among test case scenarios that are carried out indicated that the samples coated with MnO_2 layer which has dielectric value (κ) ≅ 101, as aforementioned, produced significantly high power density when compared to HfO_2 (κ ≅ 25) and Al_2O_3 (κ ≅ 9). The aforementioned comparative analysis of the considered test case scenarios paves a path in the direction of advancement in flexible electrodes based on bias-free energy-harvesting applications. It is observed that the high dielectric-coated flexible electrodes have shown a high potential to harvest energy without any external bias voltage.

V. CONCLUSION

This study employs two distinct HDMO-coated flexible electrodes to achieve REWOD principles for energy harvesting without the need for external bias voltage. The implementation involves utilizing flexible electrodes for REWOD-based energy harvesting. The voltage and current outputs from these flexible electrodes highlight significant potential for

energy harvesting via flexible electrode technologies. The proposed experiment involves bending the REWOD structure with the electrolyte enclosed between the electrodes, resulting in a power density of 476.21 μW/cm^2, which is $\approx$118 times compared to the power density attained through the nonbending REWOD modulation experiment conducted in this study. These findings indicate the prospective ability of flexible REWOD electrodes to contribute to human-motion-driven energy harvesting, without the need for additional bias voltage. In conclusion, this study presents an improvised initial stage in the development of a single electrolyte-encaptured REWOD flexing sample with the goal of characterizing arrays of REWOD structures in the near future. For the initial demonstration, test case scenarios based on a single flexing REWOD sample with HDMO layer coating are evaluated. Future endeavors will focus on creating HDMO-coated array structures involving enclosed droplets. This approach aims to enhance the contact area between the electrode and the electrolyte, leading to increased capacitance. Consequently, higher voltage and current outputs are anticipated, leading to higher generated energy.

REFERENCES

[1] P. R. Adhikari, A. B. Patwary, K. Kakaraparty, A. Gunti, R. C. Reid, and I. Mahbub, "Advancing reverse electrowetting-on-dielectric from planar to rough surface electrodes for high power density energy harvesting," *Energy Technol.*, vol. 10, no. 3, pp. 1–12, Mar. 2022.

[2] K. Xiao and C.-X. Wu, "Dynamics of droplets driven by electrowetting," 2022, *arXiv:2203.12391*.

[3] K. Kakaraparty, G. S. Hyer, E. A. Pineda, R. C. Reid, and I. Mahbub, "Theoretical modeling and experimental validation of reverse electrowetting on dielectric (REWOD) through flexible electrodes for self-powered sensor applications," in *Proc. IEEE Sensors*, Oct. 2022, pp. 1–4.

[4] T. Krupenkin and J. A. Taylor, "Reverse electrowetting as a new approach to high-power energy harvesting," *Nature Commun.*, vol. 2, no. 1, pp. 1–7, Aug. 2011.

[5] P. R. Adhikari, N. T. Tasneem, R. C. Reid, and I. Mahbub, "Electrode and electrolyte configurations for low frequency motion energy harvesting based on reverse electrowetting," *Sci. Rep.*, vol. 11, no. 1, pp. 1–13, Mar. 2021.

[6] H. Yang, S. Hong, B. Koo, D. Lee, and Y.-B. Kim, "High-performance reverse electrowetting energy harvesting using atomic-layer-deposited dielectric film," *Nano Energy*, vol. 31, pp. 450–455, Jan. 2017.

[7] H. Yang, H. Lee, Y. Lim, M. Christy, and Y.-B. Kim, "Laminated structure of Al_2O_3 and TiO_2 for enhancing performance of reverse electrowetting-on-dielectric energy harvesting," *Int. J. Precis. Eng. Manuf.-Green Technol.*, vol. 8, no. 1, pp. 103–111, Jan. 2021.

[8] N. Wuthibenjaphonchai, M. Haruta, K. Sasagawa, T. Tokuda, S. Carrara, and J. Ohta, "Wearable and battery-free health-monitoring devices with optical power transfer," *IEEE Sensors J.*, vol. 21, no. 7, pp. 9402–9412, Apr. 2021.

[9] H. Dsouza, J. Pastrana, J. Figueroa, I. Gonzalez-Afanador, B. M. Davila-Montero, and N. Sepúlveda, "Flexible, self-powered sensors for estimating human head kinematics relevant to concussions," *Sci. Rep.*, vol. 12, no. 1, pp. 1–8, Jun. 2022.

[10] N. T. Tasneem, D. K. Biswas, P. R. Adhikari, R. Reid, and I. Mahbub, "Design of a reverse-electrowetting transducer based wireless self-powered motion sensor," in *Proc. IEEE Int. Symp. Circuits Syst. (ISCAS)*, Oct. 2020, pp. 1–5.

[11] S. C. Mukhopadhyay, "Wearable sensors for human activity monitoring: A review," *IEEE Sensors J.*, vol. 15, no. 3, pp. 1321–1330, Mar. 2015.

[12] X. Zeng, R. Peng, Z. Fan, and Y. Lin, "Self-powered and wearable biosensors for healthcare," *Mater. Today Energy*, vol. 23, Jan. 2022, Art. no. 100900.

[13] H. Zhang et al., "Graphene-enabled wearable sensors for healthcare monitoring," *Biosensors Bioelectron.*, vol. 197, Feb. 2022, Art. no. 113777.

[14] X. Huang et al., "Epidermal self-powered sweat sensors for glucose and lactate monitoring," *Bio-Des. Manuf.*, vol. 5, no. 1, pp. 201–209, Jan. 2022.

[15] S. A. Pullano, V. D. Kota, K. Kakaraparty, A. S. Fiorillo, and I. Mahbub, "Optically unobtrusive zeolite-based dry electrodes for wearable ECG monitoring," *IEEE Sensors J.*, vol. 22, no. 11, pp. 10630–10639, Jun. 2022.

[16] M. A. Mohammed, F. F. Mustafa, and F. I. Mustafa, "Feasibility study for using harvesting kinetic energy footstep in interior space," in *Proc. 11th Int. Renew. Energy Congr. (IREC)*, Oct. 2020, pp. 1–4.

[17] M. Ferrari, V. Ferrari, D. Marioli, and A. Taroni, "Modeling, fabrication and performance measurements of a piezoelectric energy converter for power harvesting in autonomous microsystems," *IEEE Trans. Instrum. Meas.*, vol. 55, no. 6, pp. 2096–2101, Dec. 2006.

[18] D. J. Apo, M. Sanghadasa, and S. Priya, "Low frequency arc-based MEMS structures for vibration energy harvesting," in *Proc. 8th Annu. IEEE Int. Conf. Nano/Micro Eng. Mol. Syst.*, Apr. 2013, pp. 615–618.

[19] A. Quattrocchi, F. Freni, and R. Montanini, "Power conversion efficiency of cantilever-type vibration energy harvesters based on piezoceramic films," *IEEE Trans. Instrum. Meas.*, vol. 70, pp. 1–9, 2021.

[20] T. Ruan, Z. J. Chew, and M. Zhu, "Energy-aware approaches for energy harvesting powered wireless sensor nodes," *IEEE Sensors J.*, vol. 17, no. 7, pp. 2165–2173, Apr. 2017.

[21] W. Peng and S. Du, "The advances in conversion techniques in triboelectric energy harvesting: A review," *IEEE Trans. Circuits Syst. I, Reg. Papers*, vol. 70, no. 7, pp. 3049–3062, Mar. 2023.

[22] E. Kovalska et al., "Textile beeswax triboelectric nanogenerator as self-powered sound detectors and mechano-acoustic energy harvesters," *Nano Energy*, vol. 120, Feb. 2024, Art. no. 109109.

[23] J. He, Y. Liu, D. Li, K. Yao, Z. Gao, and X. Yu, "Stretchable triboelectric nanogenerators for energy harvesting and motion monitoring," *IEEE Open J. Nanotechnol.*, vol. 1, pp. 109–116, 2020.

[24] C. Wu, H. Huang, S. Yang, and G. Wen, "Pagoda-shaped triboelectric nanogenerator with high reliability for harvesting vibration energy and measuring vibration frequency in downhole," *IEEE Sensors J.*, vol. 20, no. 23, pp. 13999–14006, Dec. 2020.

[25] A. Roy et al., "A 6.45 uW self-powered SoC with integrated energy-harvesting power management and ULP asymmetric radios for portable biomedical systems," *IEEE Trans. Biomed. Circuits Syst.*, vol. 9, no. 6, pp. 862–874, Dec. 2015.

[26] E. Shahhaidar, O. Boric-Lubecke, R. Ghorbani, and M. Wolfe, "Electromagnetic generator: As respiratory effort energy harvester," in *Proc. IEEE Power Energy Conf. Illinois*, Feb. 2011, pp. 1–4.

[27] C. J. Lukas et al., "A 1.02 μW battery-less, continuous sensing and post-processing SiP for wearable applications," *IEEE Trans. Biomed. Circuits Syst.*, vol. 13, no. 2, pp. 271–281, Apr. 2019.

[28] C. Zhang, Y. Jin Zhou, Q. X. Xiao, L. Yang, T. Y. Pan, and H. F. Ma, "High-efficiency electromagnetic wave conversion metasurfaces for wireless energy harvesting," in *Proc. Prog. Electromagn. Res. Symp. (PIERS)*, 2016, pp. 1720–1722.

[29] B. Andò, S. Baglio, V. Marletta, and A. R. Bulsara, "Modeling a nonlinear harvester for low energy vibrations," *IEEE Trans. Instrum. Meas.*, vol. 68, no. 5, pp. 1619–1627, May 2019.

[30] J. J. L. Aranda, S. Bader, and B. Oelmann, "An apparatus for the performance estimation of pressure fluctuation energy harvesters," *IEEE Trans. Instrum. Meas.*, vol. 67, no. 11, pp. 2705–2713, Nov. 2018.

[31] S. Hu et al., "A stretchable multimode triboelectric nanogenerator for energy harvesting and self-powered sensing," *Adv. Mater. Technol.*, vol. 7, no. 3, 2022, Art. no. 2100870.

[32] S. Sankar, P.-H. Chen, and M. S. Baghini, "An efficient inductive rectifier based piezo-energy harvesting using recursive pre-charge and accumulation operation," *IEEE J. Solid-State Circuits*, vol. 57, no. 8, pp. 2404–2417, Aug. 2022.

[33] Y. C. Shu and I. C. Lien, "Analysis of power output for piezoelectric energy harvesting systems," *Smart Mater. Struct.*, vol. 15, no. 6, pp. 1499–1512, Sep. 2006.

[34] U. Laurentiu, C. Romeo, S. Cristina, M. Aradoaei, P. Olga, and M. Baibarac, "Flexible piezo-electric composites for 3D-printed harvesters," in *Proc. Int. Conf. Expo. Electr. Power Eng. (EPE)*, Oct. 2020, pp. 470–473.

[35] W. Xu et al., "A droplet-based electricity generator with high instantaneous power density," *Nature*, vol. 578, no. 7795, pp. 392–396, Feb. 2020.

[36] H. Zheng et al., "Remote-Controlled droplet chains-based electricity generators," *Adv. Energy Mater.*, vol. 13, no. 10, Mar. 2023, Art. no. 2203825.
[37] T.-H. Hsu, S. Manakasettharn, J. A. Taylor, and T. Krupenkin, "Bubbler: A novel ultra-high power density energy harvesting method based on reverse electrowetting," *Sci. Rep.*, vol. 5, no. 1, pp. 1–13, Nov. 2015.
[38] D. H. Huynh et al., "Environmentally friendly power generator based on moving liquid dielectric and double layer effect," *Sci. Rep.*, vol. 6, no. 1, pp. 1–10, Jun. 2016.
[39] P. R. Adhikari, M. N. Islam, Y. Jiang, R. C. Reid, and I. Mahbub, "Reverse electrowetting-on-dielectric energy harvesting using 3-D printed flexible electrodes for self-powered wearable sensors," *IEEE Sensors Lett.*, vol. 6, no. 5, pp. 1–4, May 2022.
[40] K. Kakaraparty, E. A. Pineda, R. C. Reid, and I. Mahbub, "Advancement of reverse electrowetting-on-dielectric with flexible electrodes for bias-free Energy- harvesting applications," *IEEE Sensors J.*, vol. 23, no. 10, pp. 10334–10341, May 2023.
[41] S. C. Chandrarathna and J.-W. Lee, "16.8 nW ultra-low-power energy harvester IC for tiny ingestible sensors sustained by bio-galvanic energy source," *IEEE Trans. Biomed. Circuits Syst.*, vol. 15, no. 1, pp. 55–67, Feb. 2021.

Karthik Kakaraparty (Graduate Student Member, IEEE) is currently pursuing the Ph.D. degree with the Electrical and Computer Engineering Department, The University of Texas at Dallas, Richardson, TX, USA, under the supervision of Dr. Ifana Mahbub.

His current research interests include antenna designs for applications related to millimeter waves, 5G technologies, REWOD energy harvesting based on flexible electrodes, and antenna designs for on-body flexible electronics-based applications.

Erik A. Pineda is currently pursuing the master's degree in electrical engineering with the University of Texas at Dallas, Richardson, TX, USA.

He enjoys working with technology, software integration, and hardware manipulation. He is currently with the iBioRFCASL, Department of Electrical Engineering, University of Texas at Dallas, as a Research Assistant of Software Components.

Baylee Schumacher is currently pursuing the bachelor's degree in mechanical engineering with Utah Tech University, St. George, UT, USA. Her academic pursuits have developed a strong passion for material science, prototyping, manufacturing, and the complexities of high-level physics.

As she takes her first steps into the field of research, she is particularly captivated by the potential of REWOD energy harvesting on flexible electrodes and printable circuit technology.

Russell C. Reid received the bachelor's degree from Brigham Young University, Provo, UT, USA, in 2003, the master's degree from the University of Virginia, Charlottesville, VA, USA, in 2005, and the Ph.D. degree from The University of Utah, Salt Lake City, UT, USA, in 2016.

He is an Assistant Professor with the Department of Engineering, Utah Tech University, St. George, UT, USA. He was previously an Assistant Professor of Mechanical and Energy Engineering with the University of North Texas, Denton, TX, USA. He has been or is currently the PI or Co-PI on federally funded grants as well as internally funded university grants. He has also been heavily involved in the development of the Engineering Department, Utah Tech University. His research interests include energy harvesting, biosensors, and electrowetting.

Ifana Mahbub (Senior Member, IEEE) is an Assistant Professor and the Texas Instrument's Early Career Chair Awardee of the Department of Electrical and Computer Engineering, The University of Texas at Dallas, Richardson, TX, USA, where she is leading the Integrated Biomedical, RF Circuits and Systems Laboratory (iBioRFCASL). She has published two book chapters, 29 journal publications, and over 62 peer-reviewed conference publications. Her research interests include energy-efficient integrated circuits and systems design for read-out, wireless communication, wireless power transfer for various implantable and wearable sensors, and ultrawideband/mm-wave phased-array antenna design for far-field wireless power transfer/V2V communication for UAVs.